2007 IEEE International Conference on
Robotics and Automation
Roma, Italy, 10-14 April 2007

M³: Multiscale, Deterministic and Reconfigurable Macro-Micro Assembly System for Packaging of MEMS

Rakesh Murthy, Aditya N. Das, Dan Popa, and Harry Stephanou

Abstract— This paper presents recent results in configuring a multiscale (macro-micro) robotic assembly platform with modular and reconfigurable characteristics. M³ is a multi-robot system capable of spanning across the macro-meso-micro scales, and has been specifically designed to package MOEMS (Micro Opto Electro Mechanical Systems). The emphasis on packaging (as opposed to assembly) is inclusive of the latter, but it also recognizes that bonding, sealing and attachment processes must also be controlled, and will greatly influence the reliability of the microsystem. The system components include precision robots, microstages, end-effectors and fixtures that accomplish assembly tasks in a shared workspace. The system components are systematically characterized in terms of accuracy and repeatability, and assembly plans are performed using kinematic identification, visual servoing, inverse kinematics, and dynamic vibration suppression. As an application packaging problem, various micro and meso scale parts are assembled into a MEMS device. The tolerance budget of assembly ranges from 4 microns to 300 microns, while the size of components in the assembly ranges from 126 microns to 30mm. Various end-effectors and fixtures have been designed for use with off-the-shelf hardware (robots and microstages) and were tested for precision performance. The robots are calibrated to accuracies of 10 microns or less. In this paper we present experimental results of precision robot calibration and visual servoing for fiber pigtailing with one of the robots within M³.

I. INTRODUCTION

Over the past decade, with the emergence of heterogeneous microsystems, such as optical and fluidic MEMS, numerous precision systems have been employed for higher volume manufacturing of these devices [1-8]. These systems can be classified in multiple ways, such as on the basis of throughput (serial, parallel), type of end-effectors (contact, non-contact), and level of human intervention (manual, teleoperated or automated) [1, 7-8]. Nevertheless, assembly and packaging at the micro scale remains highly challenging and requires bridging the gap between multiple scales of tolerance, part dimension, and workspace limitations. Given the multiscale nature of MEMS, assembly and packaging systems such as the one presented in this paper are clearly necessary to achieve low-cost prototyping and pilot production.

Due to the increased demand for Micro-Opto-Electro-Mechanical System (MOEMS), automated microassembly platforms for such devices have been receiving special attention. Applications include automated assembly for fiber-optics and micro-optical components into devices such as micro-optical benches, WDM (wavelength division multiplexing) components, 1xN and NxN fiber arrays, etc. Recently, a multitude of commercially available and custom equipment has been developed for fiber optic handling, in particular fiber arrays, fixtures, alignment systems, spooling, stripping, etc. [13-16].

In general, commercially available equipment is expensive, lacks versatility, modularity and reconfigurability. Such equipment is often configured for a specific product, process or hardware vendor, requires extensive calibration and the intervention of human operators during assembly. The absence of open-architecture, general-purpose micropackaging systems has contributed to the high cost of MEMS according to the following *OP³ law: one product, one process, one piece of equipment (our definition).* In order to produce microsystems such as MEMS, MOEMS or microfluidic devices, microassembly alone is not sufficient, i.e., it must be combined with other processes, in particular joining, bonding and sealing.

In this paper we describe advances in the coordination and control within the M^3, a multiscale robotic assembly and packaging system developed at the Automation & Robotics Research Institute at the University of Texas Arlington. This system builds upon previous work [3, 7], is modular and reconfigurable, can operate across multiple scales (Macro-Meso-Micro=M^3) and is currently being used in pilot production of heterogeneous MEMS devices such as the one shown in Figure 1. Typical assembly and packaging operations currently supported by M³ include precision die and package manipulation, die attach, optical fiber handling, precision fiber pigtailing, and laser solder reflow in inert environments.

Included in the objectives of our work are incorporating modularity and reconfigurability into the mechanical design and the system software, so that we can reuse the system for

Manuscript received January 31, 2007. This work was supported by the Office of Naval Research under grant # N00014-04-1-0611. The authors are with the Automation and Robotics Research Institute (ARRI), at the University of Texas at Arlington, Fort Worth, TX 76118 USA.

Aditya N. Das and Rakesh Murthy are pursuing their doctorate studies in Electrical Engineering with Professor Popa at ARRI, UT Arlington, in the area of multiscale robotics.

Dan O. Popa, Ph.D., (also corresponding author) is currently an Assistant Professor of Electrical Engineering with the Automation & Robotics Research Institute at the University of Texas at Arlington, Fort Worth, TX 76118 USA (e-mail: popa@arri.uta.edu). His research interests include multiscale and microrobotics, 3D microsystems integration, embedded and distributed sensors and actuators.

Harry Stephanou, Ph.D. is Professor of Electrical Engineering and Director of the Automation & Robotics Research Institute at the University of Texas at Arlington. His research interests include small-scale robotics and distributed robotic systems.

different applications. The key to reusability is the systematic characterization of the system accuracy, resolution and repeatability, combined with appropriate multiscale fixturing, end-effector design, kinematic identification and closed-loop servoing [10, 11].

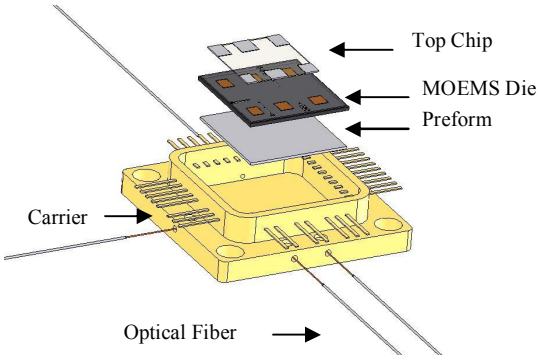

Fig.1. Components of a MOEMS Package

The paper is organized as follows: in Section 2 we describe the M³ hardware and software architecture; in Section 3 we describe kinematic identification (calibration) of one of the robots in the workspace; in Section 4 we experimentally demonstrate fiber pigtailing using visual servoing; finally section 5 concludes the paper.

II. M³ SYSTEM ARCHITECTURE

In order to perform multiscale assembly, a consistent approach to the design of fixtures, end-effectors, and software algorithms was followed. Two iterative loops that generate improvements based on accuracy measurements and on the assembly yield are depicted in Figure 2.

Within M³, the types of assembly and packaging operations supported target the packaging of heterogeneous MOEMS devices such as the one shown in Figure 1. These micro and meso-scale parts include a Kovar® carrier package and lid, four optical fibers fed through the carrier, a silicon MEMS die, a glass cap die, wire-bonds, and several solder preforms. Assembly operations include (1) precision pick and place of components such as package, MEMS die and solder preforms from a parts tray to a hotplate; (2) optical fiber handling and insertion into package and DRIE MEMS trenches; and (3) preform handling and laser positioning for soldering in inert gas environment to attach the fibers to the package.

During packaging, two types of challenges needed to be addressed: the automated mechanical handling of all microcomponents at different levels of accuracy, and the integration of reliable attachment and sealing processes into the micromanufacturing process. To accomplish the required tasks, the M³ uses many robotic subsystems that aid coarse-fine motion and machine vision. A total of four precision robots share a large, macro-scale workspace (several ft³). Three of the robots (called pucks) are mobile on an inverted air-bearing surface as depicted in Figure 3.

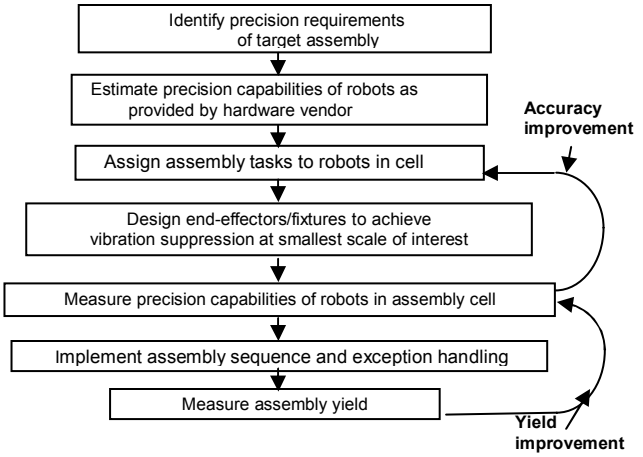

Fig. 2. Schematic diagram of methodology for designing a multiscale assembly system

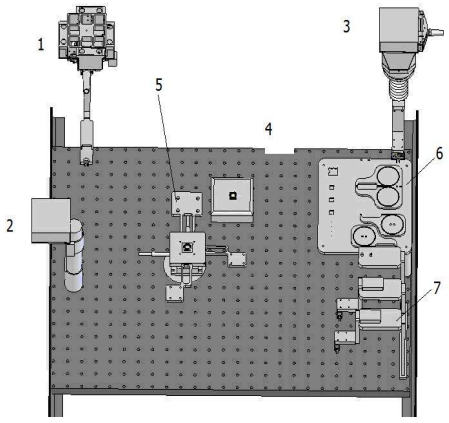

Fig.3. M³ hardware: (1) Three axis XYZ (R_4) robot ; (2) Four axis XYZθ (R_1) robot; (3) Four axis XYZθ (R_2) robot; (4) Optic Breadboard; (5) Four axis XYZθ (R_3) robot; (6) Parts tray; (7) Tool rest

Within M³, the air-bearing system we use is Motoman's Robotworld® hardware. To these pucks we attach additional degrees of freedom and custom, interchangeable end-effectors. The robots are a coarse positioning puck (R_2), a mobile motorized zoom microscope fine positioning puck (R_1), a coarse positioning puck for a reflow laser (R_4), and a custom fine positioning manipulator (R_3) for optical fiber handling. Several end-effectors are picked up from a tool rest via a pneumatic tool changer by manipulator R_2, while R_3 is constructed using discrete stages from other hardware vendors. For a more complete description of M³ see our previous publication [10].

To coordinate and control the operation of the multiscale robotic platforms and to automate the assembly, modular software applications are run in supervisory mode from central PCs. These software modules are written in Labview ™ and provide an interactive user interface, such as

the one shown in Figure 4 that provides direct user access to subsystems, algorithms and process monitors. The system software manages manipulator calibration, kinematics, trajectory planning, assembly and packaging sequence execution and machine vision for "look-and-move" visual servoing.

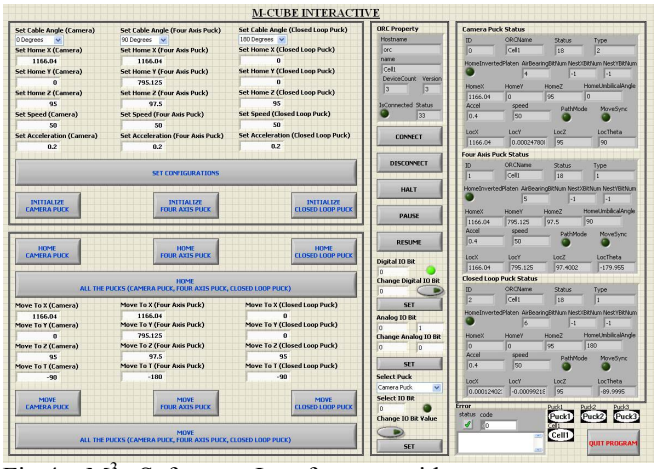

Fig.4. M^3 Software Interface provides user access to different modules like calibration, assembly sequence execution and machine vision

In architecting the system software architecture, we aimed to support changes in tooling, end-effector kinematics, number of end-effectors, modified assembly sequences, and the addition of sensors. The modules of the supervisory software include (1) Robot Control Module; (2) Vision Control Module; (3) Motion Control; (4) Calibration Module; (5) Automation Module; (6) Status Monitoring.

The Robot Control module configures and controls individual robotic manipulators. Robots R_1-R_4 are abstracted and specified into a sub-VI that provides direct access to low-level commands. The Vision Control module aids in the attaining the required system precision and is also used to monitor the assembly process. Proper operation of the motorized stages, motorized zoom control for the microscopes and control for pneumatic and vacuum grippers such as solenoid and relay controls are governed by the Motion Control module. The Calibration Module is responsible in system calibration. Calibration point selection and generation are managed by this VI. Automation of the assembly process requires implementation of the assembly plan, trajectory planning, collision avoidance, inverse kinematics, tolerance analysis and accuracy measures, which are provided through programming in the Automation Module.

III. KINEMATIC CALIBRATION FOR ROBOT R_3

In order to design and characterize the multiscale robotic platform to perform assembly, a systematic approach is adopted. For the MEMS assembly in Figure 1, the tolerance budget is detailed in [10] and contains values between 4 µm for fiber into MEMS trench insertion, and 300 µm for fiber-into-package insertion. This budget restricts acceptable manipulator errors in positioning.

Next, the actual accuracy and repeatability of the manipulators is directly measured and/or compared to the hardware vendor specifications. For example, the zoom microscope accuracy and repeatability is experimentally determined through statistical experimentation. The M^3 robots are XY accurate to values between 8 and 51.78 microns respectively taken in different points of their workspace. In case of a reconfigurable end-effector, the robot accuracy is measured by initializing, picking up a suitable tool, an assembly component with the tool and positioning it at a desired target location in the workspace. These measurements are carried out using zoom microscopes and repeatability is measured when the robot switches between two locations with the "to be assembled" component in grasped condition.

Finally, with complete information related to the allowable tolerances and the precision capability, we make an assembly plan. This involves assigning suitable tasks for each robot, and determining the exact balance between fixturing, calibration and servoing, according to the following set of rules: (a) Fixtures can be used to locate objects in the assembly space only when the manipulator accuracy is smaller than the required tolerance; (b) Calibration can be used to locate objects in the workspace only when the repeatability of the manipulator is smaller than the required tolerance; (c) Servoing (for instance visual servoing) on relative position can be used only if the resolution of the manipulator is smaller than the required tolerance. For example, MEMS die positioning which involves a tolerance of 50 microns inside the carrier requires calibration, while the positioning of optical fibers onto the die with allowable tolerance of 4 microns requires a combination of calibration and visual servoing. The complete robot assignment for both systems is based on minimal positioning and process precision needs and thus avoids over-design of the assembly cell.

Coordination within the M^3 system workspace is accomplished by expressing the local coordinate frames attached to each robot in a single global frame, attached to Robotworld®'s platen. In past work [10] we detailed calibration and inverse kinematics for robot R_2 during die pick-and-place operations. The Kinematic ID, and visual servoing with procedure followed for the R_3 robot, the one carrying fibers and fiber spools, is detailed in the remainder of this paper. R_3 is used as a carrying platform for a fixture referred to as a "fiber spool platform". Fiber spools are fixtures containing 2 ft long optical fibers wrapped around in a tight space. A fiber gripper located on the R_2 robot is used to hold fibers in place, while R_3 aligns the fiber into corresponding MEMS trenches as shown in Figures 5 and 6.

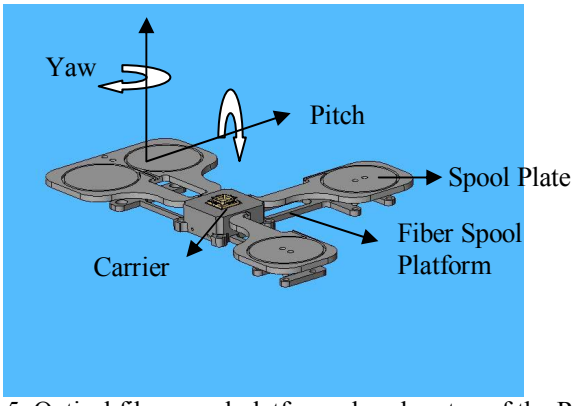

Fig.5. Optical fiber spool platform placed on top of the R_3 XYZθ robot

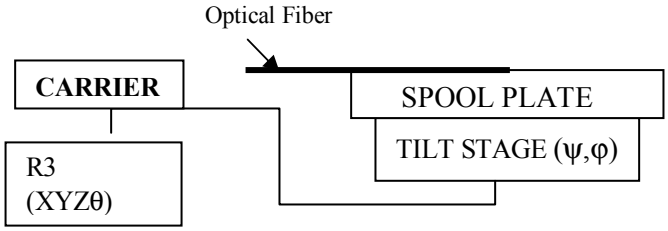

Fig.6. Line Diagram showing optical fiber fixturing

The local coordinate frame associated with R_3 is in encoder counts and is rotated and transformed with respect to the global coordinate (platen) frame. A gray box kinematic model for this robot is of the form:

$$\begin{bmatrix} X \\ Y \end{bmatrix}_{global} = G_{2x2}.l.\left(\begin{bmatrix} E_x \\ E_y \end{bmatrix} + \begin{bmatrix} K_1 \\ K_2 \end{bmatrix}\right) + \begin{bmatrix} R_{3x} \\ R_{3Y} \end{bmatrix} + R_3(\theta)_{(2x2)}[M_{1_{(2x2)}} \quad T_{(2x1)}]\begin{bmatrix} P_{xinit} \\ P_{yinit} \end{bmatrix} \quad (1)$$

Where $G \in SO(2)$ is a rotation matrix along the common Z axis between the two coordinate frames (R_3 and global). 'l' is the multiplication factor from encoder counts to millimeters. [E_x, E_y] are the X and Y axes encoder counts. [K_1 K_2] are the displacement parameters to be estimated from R_3 local coordinate frame. [R_{3x} R_{3y}] are the position of the R_3 coordinate axis origin in global coordinates. $R_3(\theta)$ is the rotation matrix corresponding to the θ axis on the robot. M_1 is a 2x2 transformation matrix for the R_1 robot. T is a 2x1 vector relates to offsets in displacement caused due to rotation 'θ'. To estimate the product (G.l), we start by actuating only the X,Y servos on the R_3 robot while observing the motion with the microscope zoom camera mounted on R_1. This robot is itself calibrated with respect to the platen as in [10]. By taking repeated measurements, we can determine the location of a reference point in global coordinates.

Taking the differences between consecutive readings with a constant θ angle, e.g. subtracting equations of type (1) from each other, we get simply:

$$\begin{bmatrix} \Delta X_n \\ \Delta Y_n \end{bmatrix}_{global} = G_{2x2}.l.\begin{bmatrix} \Delta E_{xn} \\ \Delta E_{yn} \end{bmatrix} \quad (2)$$

Or

$$\begin{bmatrix} \Delta X_n \\ \Delta Y_n \end{bmatrix}_{global} = \begin{bmatrix} g_{11} & g_{12} \\ g_{21} & g_{22} \end{bmatrix}\begin{bmatrix} \Delta E_{xn} \\ \Delta E_{yn} \end{bmatrix} \quad (3)$$

Rewriting this equation as a linear LSQ equality, we obtain:

$$\begin{bmatrix} \Delta E_{x1} & \Delta E_{Y1} & 0 & 0 \\ 0 & 0 & \Delta E_{x1} & \Delta E_{Y1} \\ . & & & \\ . & & & \\ \Delta E_{xn} & \Delta E_{Yn} & 0 & 0 \\ 0 & 0 & \Delta E_{xn} & \Delta E_{Yn} \end{bmatrix}\begin{bmatrix} g_{11} \\ g_{12} \\ g_{21} \\ g_{22} \end{bmatrix} = \begin{bmatrix} \Delta X_1 \\ \Delta Y_1 \\ . \\ . \\ \Delta X_n \\ \Delta Y_n \end{bmatrix} \quad (4)$$

Tables 1 and 2 show sample measurements (i.e. global coordinates estimated by the camera, and encoder readings) by observing the same feature on the MEMS die while robot R_3 is moving.

TABLE 1. EXPERIMENTAL GLOBAL COORDINATES SHOWN AT ONLY 4 POINTS CORRESPONDING TO EQUATION (1)

Location	X_{global} (mm)	Y_{global} (mm)
1	813.76	429.48
2	815.3	429.48
3	816.36	429.48
4	816.39	431

TABLE 2. ENCODER VALUES OF R_3 FOR POINTS MEASURED IN TABLE 1.

Location	Ex (counts)	Ey(counts)
1	0	0
2	-25000	0
3	-42000	0
4	-42000	25000

Substituting the data shown in Tables 1 and 2 into equation (4) and using a linear least squares fit on the data, the following G.l matrix;

$$G.l = \begin{bmatrix} -6.2071e & -005 & 1.3089e & -006 \\ 7.2072e & -008 & 6.1393e & -005 \end{bmatrix}$$

Referring back to Equation (1), the unknown parameters that still need identification are: [k1 k2] and [t1 t2]. We now take X, Y and also θ increments with robot R3 to determine the remaining unknowns also via difference measurements. Using experimental data in Equation (5) and fitting a linear equation between the data, we arrive at the following parameters (using 9 datapoints):

$$k_1 = 789.9662, k_2 = 431.994, t_1 = 21.9762, t_2 = 2.5694$$

The identification of these parameters is validated by determining the repeatability of R_3 between two points referenced using R_1. The resulting distribution had an associated variance of 4.9 μm in X and Y. To improve on this figure, we used a set of 30 datapoints in the kinematic

identification procedure that resulted in the following parameters

$k_1 = 789.9872, k_2 = 430.23, t_1 = 21.9762, t_2 = 2.5684$

$$[Gl \quad R_3(\theta_i)]\begin{bmatrix} k1 \\ k2 \\ t1 \\ t2 \end{bmatrix} = \begin{bmatrix} X_i \\ Y_i \end{bmatrix} - G.l.\begin{bmatrix} E_{xi} \\ E_{yi} \end{bmatrix} - R(\theta_i)M_1\begin{bmatrix} P_{xinit} \\ P_{yinit} \end{bmatrix}$$

$$\begin{bmatrix} Gl & R_3(\theta_1) \\ Gl & R_3(\theta_2) \\ ..... & \\ ..... & \\ ..... & \\ Gl & R_3(\theta_n) \end{bmatrix}\begin{bmatrix} k1 \\ k2 \\ t1 \\ t2 \end{bmatrix} = \begin{bmatrix} f(X_1, Y_1, \theta_1) \\ f(X_2, Y_2, \theta_2) \\ .... \\ .... \\ .... \\ f(X_n, Y_n, \theta_n) \end{bmatrix} \quad (5)$$

With these parameters, the calibrated R_3 was repeatable with 4.1 μm variance. Following calibration, R_3 is used to perform fiber insertion, as detailed in the next section.

IV. VISUAL SERVOING WITH ROBOT R_3

To accomplish fiber insertion using visual servoing of robot R_3 we used the following sequence:

- Using an inverse kinematic solution, the fiber is inserted into the feedthrough hole inside the carrier.
- Optical fiber insertion into a DRIE trench is guided by via points through which the fiber tip is aligned for insertion.
- Next, we use an image based Jacobian that relates changes in image features (pixels) to corresponding change in robot encoder space, as shown in equation (11). The pixel error vector $[\Delta P_x, \Delta P_y, \Delta\theta]'$ is used to calculate the required joint actuation vector $[\Delta E_x, \Delta E_y, \Delta\theta_o]'$ for the robot R_3.
- R_3 is commanded to execute the positioning correction given by $[\Delta E_x, \Delta E_y, \Delta\theta_o]$.
- The above outlined procedure is executed in a loop to guide the fiber to follow a trajectory defined by imaging the trench and fiber repeatedly.

E_x, E_y and θ_o are the joint coordinates of M³ manipulator R_3, and X_p, Y_p and θ_p are the position and orientation of the fiber tip in global coordinates. The relationship between the pixel measurements using the zoom camera (P_x, P_y) and the location of the fiber in global coordinates is determined by

$$\begin{bmatrix} X_p \\ Y_p \end{bmatrix} = G_{2x2}.l.\left(\begin{bmatrix} E_x \\ E_y \end{bmatrix} + \begin{bmatrix} K_1 \\ K_2 \end{bmatrix}\right) + \begin{bmatrix} R_{3x} \\ R_{3Y} \end{bmatrix} + R_3(\theta)_{(2x2)}[M_{1_{(2x2)}} \quad T_{(2x1)}]\begin{bmatrix} P_{xinit} \\ P_{yinit} \end{bmatrix},$$

$$\theta_p = \theta_o + \theta_{offset} \quad , \quad (6)$$

Where M_1 is a 2x2 calibration matrix for the R_1 robot [10], $R(\theta_0)$ is the unitary rotation matrix of angle θ_o, t_1, t_2, k_1, k_2, θ_{offset} are unknown constants and P_{xinit}, P_{yinit} are the initial pixel vector of the fiber tip. The kinematic identification procedure described in section III has been used to estimate these constants from repeated measurements using a 3x3 grid.

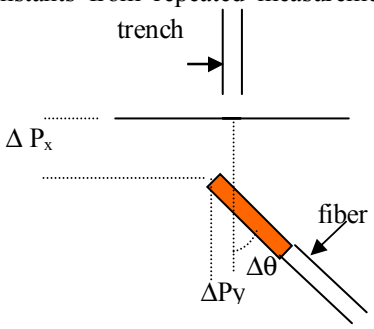

Fig.7. Alignment offset calculation in pixel coordinates

At the same time, the R_1 manipulator used for imaging yields:

$$\begin{bmatrix} X_p \\ Y_p \end{bmatrix} = \begin{bmatrix} X_c \\ Y_c \end{bmatrix} + M_1\begin{bmatrix} P_x \\ P_y \end{bmatrix} \quad (7)$$

in which, X_c, Y_c are the camera R_1 (X, Y) joint coordinates. The measured calibration data were:

[Pxinit, Pyinit] = [123.792, 129.495];

M_1= [0.011654, -0.000094011; 0.00016128,-0.011695];

We now use these constants to calculate the image Jacobian corresponding to the R_3 manipulator and use it to guide the fiber into the trench using visual servoing. To calculate the Jacobian, relate small changes in joint R_3 coordinates to small changes in pixel values for the fiber tip from equations (6) and (7):

$$\begin{bmatrix} \Delta P_x \\ \Delta P_y \end{bmatrix} = M_1^{-1}\left[G_{2x2}l\begin{bmatrix} E_x \\ E_y \end{bmatrix} + \begin{bmatrix} -\sin(\theta_o) & -\cos(\theta_o) \\ \cos(\theta_o) & -\sin(\theta_o) \end{bmatrix}\Delta\theta_o[M_{1_{(2x2)}} \quad T_{(2x1)}]\begin{bmatrix} P_{xinit} \\ P_{yinit} \end{bmatrix}\right] \quad (8)$$

or

$$\begin{bmatrix} \Delta P_x \\ \Delta P_y \end{bmatrix} = M_1^{-1}\left[G_{2x2}l\begin{bmatrix} \Delta E_x \\ \Delta E_y \end{bmatrix} + \Delta\theta_o\begin{bmatrix} b_1(\theta_o) \\ b_2(\theta_o) \end{bmatrix}\right], \quad (9)$$

in which,

$$\begin{bmatrix} b_1(\theta_o) \\ b_2(\theta_o) \end{bmatrix} = \begin{bmatrix} -\sin(\theta_o) & -\cos(\theta_o) \\ \cos(\theta_o) & -\sin(\theta_o) \end{bmatrix}\left[M_1\begin{bmatrix} P_{xinit} \\ P_{yinit} \end{bmatrix} + \begin{bmatrix} t_1 \\ t_2 \end{bmatrix}\right] \quad (10)$$

We now rearrange equation (9) as an image Jacobian:

$$\begin{bmatrix} \Delta Px \\ \Delta Py \\ \Delta\theta \end{bmatrix} = J\begin{bmatrix} \Delta E_X \\ \Delta E_Y \\ \Delta\theta_o \end{bmatrix} \quad (11)$$

Where;

$$J = \begin{bmatrix} M_1^{-1}G_{2x2}l & M_1^{-1}\begin{bmatrix} b_1(\theta_o) \\ b_2(\theta_o) \end{bmatrix} \\ 0 \quad 0 \qquad\qquad 1 \end{bmatrix} \quad (12)$$

Experimentally, we approximate the Jacobian around the origin of the rotation axis of R_3, ($\theta_o \sim = 0$), and use the

approximate Jacobian to perform visual servoing. Based on the calibration parameters we get,

$$J = J(0) = \begin{bmatrix} -0.00053272 & 6.9985e-005 & -114.62 \\ -1.3509e-005 & -0.0052483 & 509.31 \\ 0 & 0 & 1 \end{bmatrix}$$

The servoing results are shown in Figure 8. The error in positioning the fiber at the final via point (end of trench) was 2.90 μm in X and 0.01 degrees.

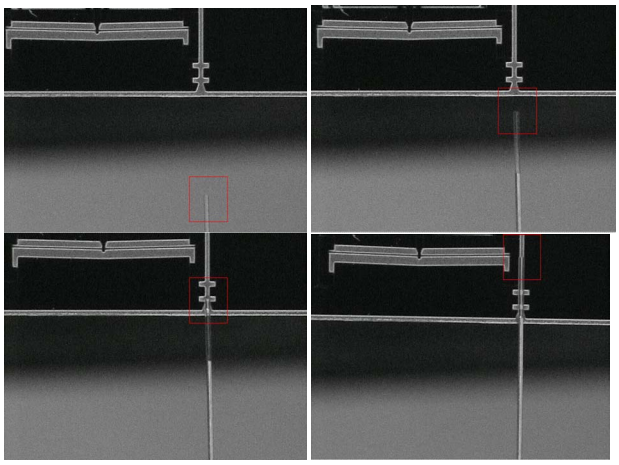

Fig.8. A 126 μm gold coated optical fiber inserted into the package and the DRIE trench. The fiber tip is highlighted in 4 different frames.

V. CONCLUSION

This paper presents M³, a robotic assembly platform with multiscale assembly and packaging capability. Even though we configured the system for packaging of a particular MOEMS device, the flexibility of this architecture makes it possible to quickly reconfigure the system for other tasks, as it is often needed in a research or a low-volume production facility. We use a rigorous approach to evaluate the tolerance budget of an assembly task, the positioning accuracy of the manipulators, tools and fixtures, and we use quantitative measures to assign manipulator tasks. We indicate how to systematically use fixtures, calibration, inverse kinematics and visual servoing to achieve the necessary levels of precision, and we present experimental results of calibration and servoing with one of the robots in the workspace. Future work will include the implementation of the assembly sequencer using a discrete event controller (DEC), and the characterization and compensation of dynamic effects (e.g. vibrations) during assembly.

REFERENCES

1. Alain Codourey, Miguel Rodriguez, Ion Pappas, "A task-oriented teleoperation system for assembly in the microworld," in Proceedings of 8th International Conference on Advanced Robotics, Monterey, CA, USA,1997.

2. T. Fukuda, F. Arai, L. Dong, "Nano robotic world - from micro to nano," in Proceedings of IEEE Conference On Robotics and Automation, Seoul, Korea, 2001.

3. D.O. Popa, B.H. Kang, J. Sin, "Reconfigurable microassembly system for photonics applications," in Proceedings of IEEE Conference on Robotics and Automation, Washington, D.C., 2002.

4. A.A. Rizzi, J. Gowdy, R.L. Hollis, "Agile assembly architecture: an agent based approach to modular precision assembly systems," in Proceedings of IEEE International Conference on Robotics and Automation, April 1997

5. S. Fatikow , J. Seyfried1 , St. Fahlbusch1 , A. Buerkle1 and F. Schmoeckel1 , "A flexible microrobot-based microassembly station," in Journal of Intelligent and Robotic Systems, Vol 27, No. 1-2, January 2000.

6. T.Hirano, K. Furata, "Micromachine technology trends in microfactory," in International Workshop on Micro-Factory (IWMF), Minneapolis, Sept 2002.

7. D.O.Popa, H.Stephanou, "Micro and meso scale robotic assembly," in SME Journal of Manufacturing Processes, Vol. 6, No.1, 2004.

8. R.Eberhardt, T. Scheller, G. Tittelbach, V. Guyenot, "Automated assembly of microoptical components," SPIE Proc. Microrobotics and Microsystems Fabrication, vol 3202, pp. 117-127, Pittsburgh, USA, 1997.

9. K. Goldberg, K.F. Bohringer, R. Fearing, "Microassembly," in Handbook of Industrial Robotics, 2nd Edition, edited by S. Nof. John Wiley and Sons, pp 1045-1066, 1999.

10. D.O. Popa, R. Murthy, J. Sin, M. Mittal, H.E. Stephanou, "M3-modular multi-scale assembly system for MEMS packaging," in Proceedings of IEEE/RSJ International Conference on Intelligent Robots and Systems, Beijing, China, October 2006.

11. D.O. Popa, M. Deeds, et. al., "Automated assembly and hermetic packaging of MOEMS for applications requiring extended self-lives," in Proceedings of ASME IMECE, November, 2005.

12. B. Nelson N.P. Papanikolopoulos, and P.K. Khosla, "Visual servoing for robotic assembly," in Visual Servoing-Real-Time Control of Robot Manipulators Based on Visual Sensory Feedback, ed. K.Hashimoto, World Scientific Publishing Co. Pte. Ltd., River Edge, NJ, pp. 139-164, 1993.

13. W.J. Shakespeare, "Optical alignment in optoelectronic components," Advancing Microelectronics, Volume 29, No. 1, January/February, 2002.

14. O. T. Strand, M. E. Lowry, "Automated fiber pigtailing technology," Electronic Components and Technology Conference, 1994, pp.1000-1003.

15. C. R. Witham, "Fiber-optic pigtail assembly and attachment alignment shift using a low-cost robotic platform," Electronic Components and Technology Conference, 2000, pp21-25.

16. S.Jang, "Automation manufacturing systems technology for opto-electronic device packaging," Electronic Components and Technology Conference, 2000.